

## Matrix-element effects in the angular-resolved photoemission from (111) silicon

Helmut Becker\* and Ulrich Gerhardt

*Physikalisches Institut der Universität Frankfurt, D-6000 Frankfurt am Main, Germany*

(Received 9 August 1978)

The angular-resolved energy-distribution functions for photoelectrons emitted from Si (111) cleavage planes are presented for plane-polarized light with photon energies below 7.1 eV at normal incidence. The spectra depend strongly on the direction of observation and on the direction of the polarization vector. A simple golden-rule expression for the number of emitted electrons is used to compare the experiments with a local-pseudopotential band-structure calculation. To interpret the results it is necessary to take into account the transition-matrix elements not only via the effect of selection rules, but by calculating them numerically.

### I. INTRODUCTION

Angular-resolved photoemission with polarized light extracts all the information that is possibly attainable by a photoemission experiment, except for the effects of spin polarization which we do not consider here. The experiments presented in this paper are done at normal incidence, since this geometry eliminates the polarization dependence described by Fresnel's formulas. Thus any polarization effects observed here must be connected with the symmetry of the electronic states involved in the photoemission process.

To interpret the observed spectra, we neglect all inelastic scattering and assume the surface to be ideal. Under these conditions, the energy and the tangential component of the wave vector are conserved in the emission of the electron. Furthermore, we calculate the number of emitted electrons using the undamped Bloch states of the volume and Fermi's golden rule. The consequence of this simple model<sup>1</sup> for the angular-resolved photoemission spectra was first discussed by Kane<sup>2</sup> to illustrate the first experimental results in this field.<sup>3</sup> Under these conditions, a structure observed in the spectra is caused by one single electronic transition between Bloch states of a specified symmetry. Thus by measuring the energy and the tangential momentum of the emitted electron, we obtain the energy and the reduced tangential wave vector of the corresponding Bloch states, i.e., the location of the transition in  $\vec{k}$  space. Furthermore, the polarization dependence of the spectra provides the remaining quantum numbers of these states.

The model described above proved to be successful in interpreting the polarization dependence of the angular-resolved photoemission from noble metals.<sup>4</sup> In this case matrix-element effects are taken into account only via group-theoretical selection rules. This is justified since the final states that contribute to the signal are dominated by one

single Fourier component. This is not the case for Si. It is therefore necessary to go beyond the selection rules and to calculate the matrix elements directly.

It is well known for Si that there are also surface states that contribute to photoemission.<sup>5</sup> However, the gross features of the result presented here seem to be dominated by volume photoemission. First experiments using Ge and Si cleavage planes were reported by Gobeli, Allen, and Kane.<sup>3</sup> These authors used polychromatic light with at most 5.8-eV photon energy. Furthermore, they could not discriminate the polar angle of emission. Nevertheless they found a strong dependence of the yield on the angle between the plane of observation and the plane of polarization. Because of the limitations in this early experiment, a comparison with theoretical band structures was not attempted. A direct comparison with our experiment is not possible, too. Because of their cleaning techniques, which include annealing, they probably had a  $7 \times 7$  surface reconstruction while we have a  $2 \times 1$  surface. Unfortunately, they also published their results only for Ge. Our results are obtained with plane-polarized monochromatic light, and the wave vector of the emitted electron is detected with respect to the azimuthal and polar angle.

In Sec. II we briefly describe the experimental setup, and present the experimental results. Finally, we analyze the results in terms of the band structure of Si and discuss the consequences of this analysis.

### II. EXPERIMENTS: METHODS AND RESULTS

Light emitted from a  $D_2$  hot filament arc discharge passes through a grating monochromator and a  $MgF_2$  senarmont polarizing prism. The two extremal positions of the polarizer subtend  $\pm 45^\circ$  with respect to the slits of the monochromator in order to minimize the polarization effect of the

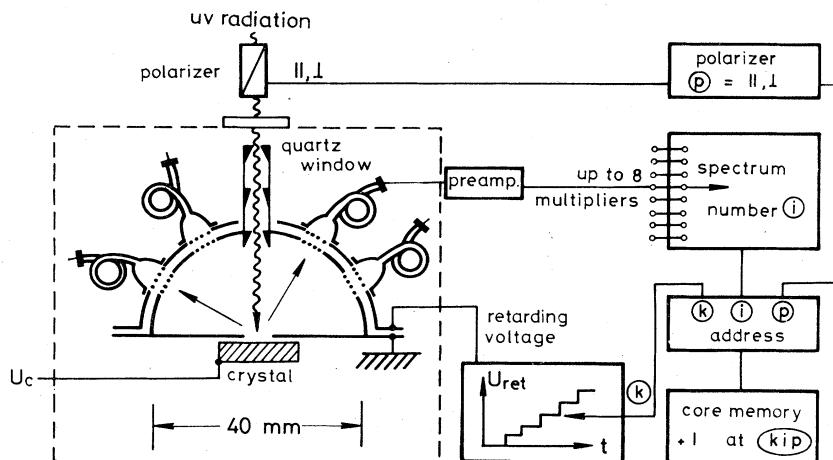


FIG. 1. Energy analyzer and data-acquisition system, both shown schematically. The address  $k i p$  refers to the step  $k$  of the retarding voltage, an electron detected by the multiplier  $i$ , with the polarizer in position  $p$ , respectively.

monochromator on the intensity of the light transmitted through the polarizer. Remaining differences in the intensities of the two polarizations are compensated by inserting a fused quartz plate into the beam. In this way the intensities for the two positions of the polarizer differ by less than  $\pm 0.5\%$ . Except for the polarizer, all optical components are made of uv grade fused quartz. The whole optical system is floated with dry nitrogen to overcome the optical absorption at  $2000 \text{ \AA}$ . The monochromator is operated at a resolution of  $0.1 \text{ eV}$  full width at half maximum. The electrostatic analyzer and the data acquisition system are shown schematically in Fig. 1; they are only slightly modified compared to the system described in Ref. 4. The photoemission system is located inside a stainless-steel ultrahigh-vacuum chamber. The base pressure of the system is below  $10^{-10}$  Torr. A Helmholtz coil is used to compensate the magnetic field of the earth. The field is reduced to values well below  $0.05 \text{ G}$ . This means that the angular deviation caused by it is below  $2^\circ$  for electrons with a kinetic energy of  $2 \text{ eV}$ . The angular resolution of the system is  $\pm 7^\circ$ . The Si crystal is cleaved *in situ* by moving simultaneously two knife edges against each other. One of the knife edges is made of cemented metal carbide, while the other one is made of Cu reinforced by a steel core. The crystal has slots on the sides facing the knife edges which are cut by a wire saw. After cutting, the sample is etched with CP6 (Ref. 6) to remove surface irregularities. Afterwards, the bottom of the slot facing the cemented metal carbide knife edge is scratched with a diamond needle.

In Fig. 2 we show the energy distribution curves for photoelectrons emitted from a Si (111) cleavage plane. The energy of the incident light is  $7.1 \text{ eV}$ . The polar angle of detection is  $30^\circ \pm 7^\circ$ . The plane of observation is the  $(1\bar{1}0)$  mirror plane in all

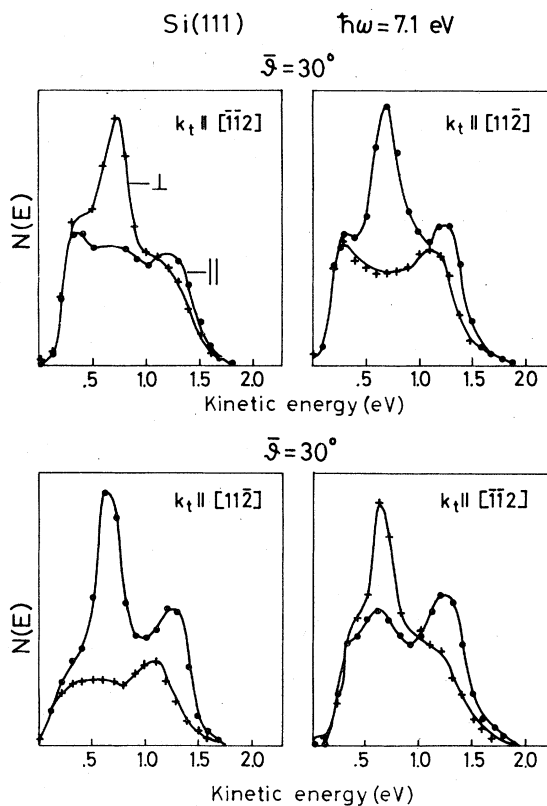


FIG. 2. Angular-resolved energy-distribution curves for a Si (111) cleavage plane obtained with  $\hbar\omega = 7.1 \text{ eV}$ . The direction of observation is  $\bar{\theta} = 30^\circ$ . The plane of detection is the  $(1\bar{1}0)$  mirror plane. The direction of  $k_t$  that is the tangential component of the wave vector is also indicated. The dots and crosses correspond to the polarization vector of the incident radiation parallel and perpendicular to the  $(1\bar{1}0)$  plane, respectively, with the radiation at normal incidence. The curves for different  $k_t$  are normalized to the same height at maximum. The lower part of the figure corresponds to a measurement after a  $60^\circ$  rotation of the sample around the  $[111]$  surface normal.

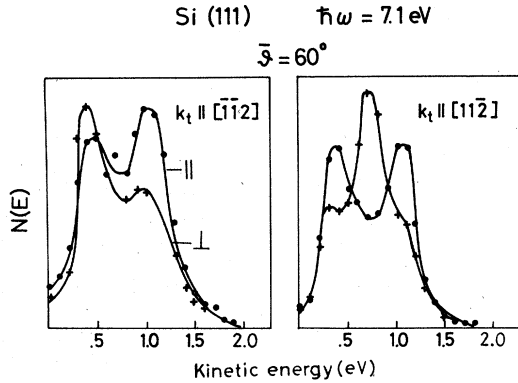


FIG. 3. Angular-resolved energy-distribution curves as in Fig. 2 except for  $\bar{\theta} = 60^\circ$ .

cases. Dots and crosses correspond to curves with the polarization vector of the incident light parallel and perpendicular to this  $(1\bar{1}0)$  plane, respectively. The direction of  $\vec{k}_t$  that is the tangential component of the wave vector is also indicated. Curves for different  $\bar{\theta}$  or  $\vec{k}_t$  are normalized to give the same height at maximum. The lower part of the figure corresponds to a measurement after a  $60^\circ$  rotation of the crystal around the  $[111]$  axis. Thus the right and left half of the figure belong to the same window and detector.

The most remarkable result is the change in the sign of the polarization effect. There is a pronounced maximum at 0.7 eV in all cases. With  $\vec{k}_t \parallel [1\bar{1}2]$ , however, it appears for the polarization vector perpendicular to the plane of observation, while for  $\vec{k}_t \parallel [112]$  the peak belongs to parallel polarization. For an ideal surface the curves shown in Fig. 2 should be crosswise identical. On the other hand, the real Si (111) cleavage plane shows a  $2 \times 1$  surface reconstruction<sup>7</sup> which might be responsible for the observed intensity variations of the spectra. The reason for these variations could also be the limited optical quality of the cleavage planes resulting in stray fields across the surface and in slight misorientations. The energetic positions of the peaks and the polarization effects, however, are reproduced quite well. Figure 3 shows typical energy distributions for a polar angle of  $60^\circ$ . Again there are strong dependences on direction and polarization. Figure 4 gives the corresponding results for  $\hbar\omega = 6.5$  eV.

### III. BAND-STRUCTURE AND MATRIX-ELEMENT ANALYSIS OF THE EXPERIMENTAL RESULTS

The golden-rule expression for the number of electrons emitted with the kinetic energy  $E$  and the tangential component  $\vec{k}_t$  of the wave vector

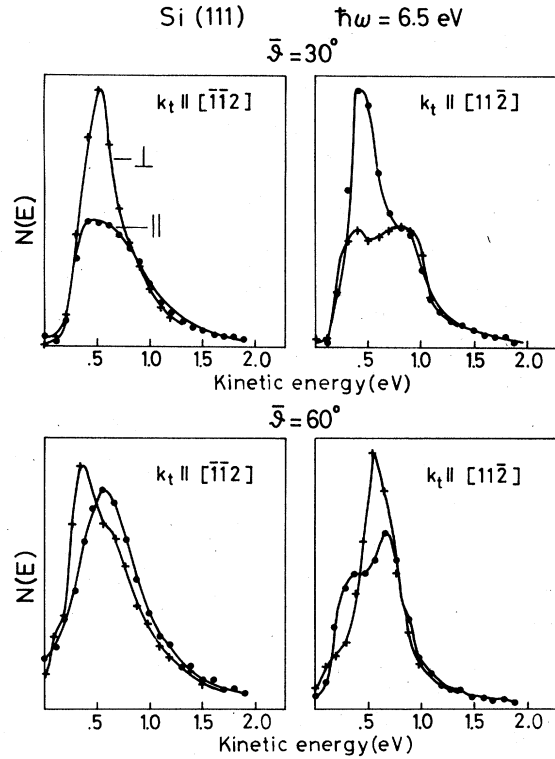


FIG. 4. Angular-resolved energy-distribution curves as in Figs. 2 and 3 except for  $\hbar\omega = 6.5$  eV.

is

$$N(\hbar\omega, E, \vec{k}) \propto \sum_{i,f} \int_{\text{BZ}} d\vec{k} |\langle f | \vec{A} \cdot \vec{p} | i \rangle|^2 \times \delta(E_{f,i}(\vec{k}) - \hbar\omega) \delta(E_f(\vec{k}) - E) \times \delta(\vec{k}_t - \vec{k}) P. \quad (1)$$

The expression  $E_{f,i}(\vec{k})$  is the energy difference between the unoccupied final state  $E_f(\vec{k})$  and the occupied initial state  $E_i(\vec{k})$ . Since  $|i\rangle = 0$  in vacuum, the integration in the transition-matrix element  $\langle f | \vec{A} \cdot \vec{p} | i \rangle$  is limited to the volume and the surface region. We neglect possible surface contributions, which is probably a good approximation for the low-energy region of our experiments where the escape depth of the electrons is still large. The first  $\delta$  function thus describes the energy and crystal momentum conservation of the optical transition between volume states. The second  $\delta$  function ensures the energy conservation in the emission process. We choose the vacuum level as the zero of the energy scale, which means that  $E$  gives the kinetic energy of the emitted electrons. The third  $\delta$  function provides for the conservation of the two-dimensional wave vector parallel to the surface, implying perfect translational symmetry along the surface. The vectors  $\vec{k}_t$  and

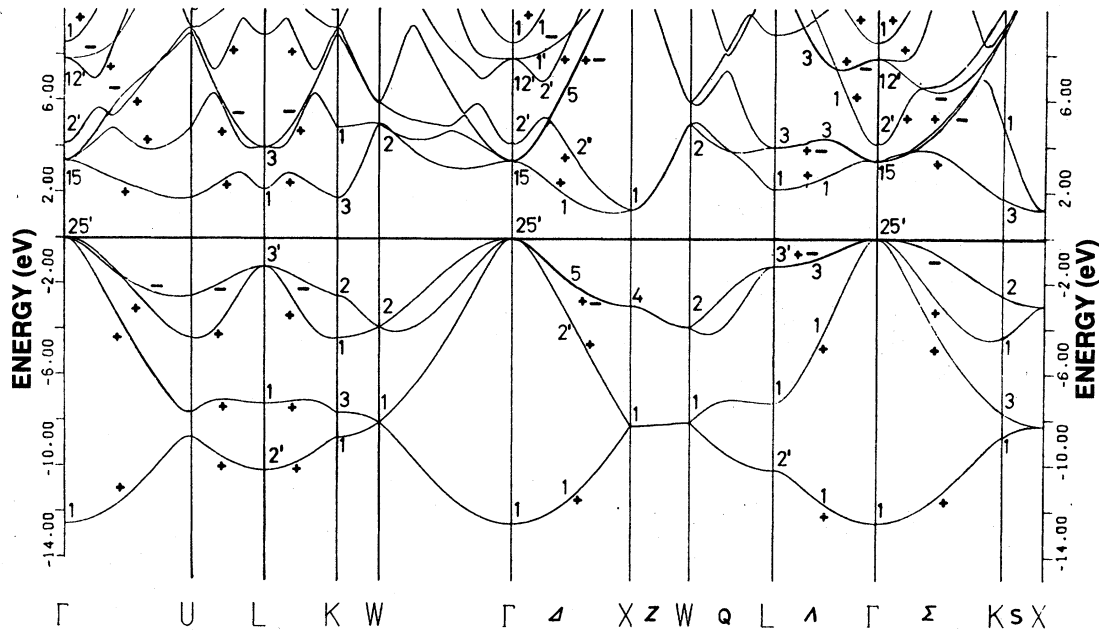


FIG. 5. Band structure of Si as calculated by Cohen and Chelikowsky. For states with  $\vec{k}$  parallel to the  $(1\bar{1}0)$  mirror plane the parity with respect to the mirror reflection is indicated by (+) and (-).

$\vec{k}$  are the tangential components of the wave vector in the crystal and in the vacuum, respectively. Finally,  $P$  is the transmission probability of the electron through the surface barrier.

The first  $\delta$  function containing constant energy differences defines the optical surface in  $\vec{k}$  space. The intersection of this surface with the surface of constant final energy given by the second  $\delta$  function defines a line in  $\vec{k}$  space along which one would have to integrate in the case of angular averaged photoemission.<sup>8</sup> In the case of angular-resolved photoemission the third  $\delta$  function restricts the contribution to a point along this line, i.e., to one particular transition. In the actual experiments, one has, of course, to work with finite energy and angular resolution, and since the number of emitted electrons is proportional to  $N(\hbar\omega, E, \vec{k})\Delta(\hbar\omega)\Delta E\Delta\vec{k}$ , one always samples the states in the neighborhood of this particular point in  $\vec{k}$  space. For the resolution used in our experiments this difference turns out to be negligible.

The dependence of the transition-matrix element on the orientation of the polarization vector  $\vec{A}$  gives rise to selection rules, provided there are symmetry operations of the crystal which leave the  $\vec{k}$  vector of the transition invariant. A particular simple and important example occurs if  $\vec{k}$  lies in a mirror plane, i.e., if the plane of detection is parallel to that mirror plane.<sup>2</sup> Since the charge density must show this mirror symmetry, the states will have either even or odd parity with

respect to the mirror reflection. The electron at the detector is a plane wave with even parity, and since the ideal surface cannot change the parity of the wave function, only electrons from final states with even parity are detected.<sup>9</sup> Correspondingly, the experiment detects even parity initial states for parallel polarization and odd parity initial

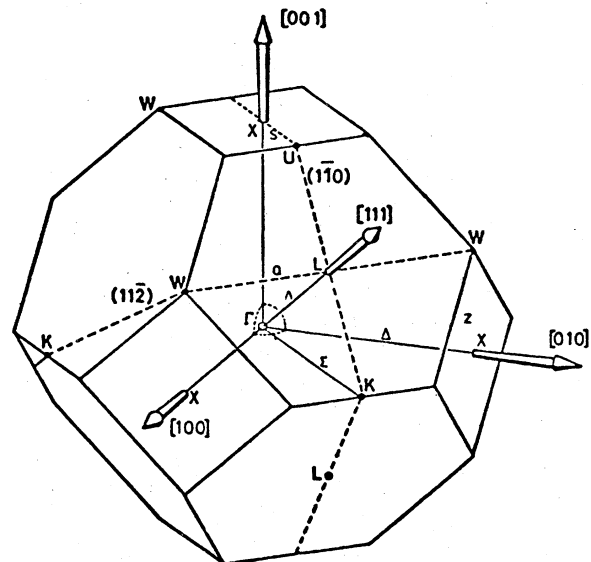


FIG. 6. fcc Bz. The dashed lines mark the  $(1\bar{1}0)$  and the  $(11\bar{2})$  plane, respectively.

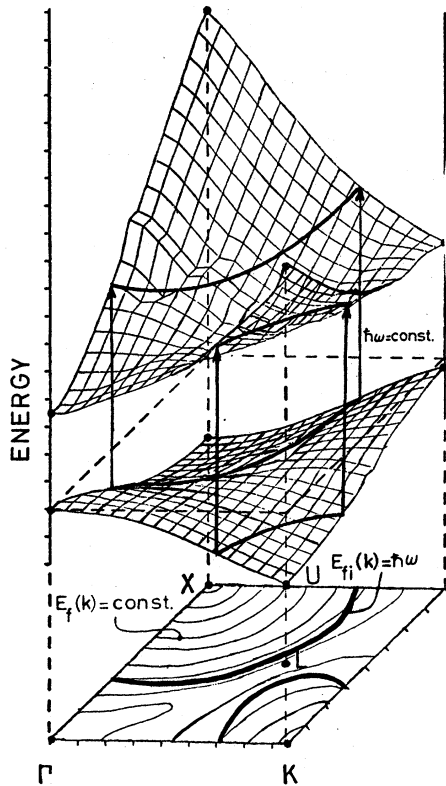


FIG. 7. Two-dimensional  $E(\vec{k})$  dependence for one valence and one conduction band. The wave vector is restricted to the  $(1\bar{1}0)$  plane. Possible optical transitions are indicated by arrows. In the lower part of the figure, the contours of constant final energies and the optical contours of constant energy difference are shown.

states for perpendicular polarization, because the matrix element is zero for an odd parity integrand. With the plane of detection parallel to the  $(1\bar{1}0)$  mirror plane, we can make use of these simple selection rules.

In order to compare quantitatively the experiment with theory, one has to calculate the band structure of Si together with the eigenstates throughout the Brillouin zone (BZ). We therefore reproduce a pseudopotential band-structure calculation of Chelikowsky and Cohen.<sup>10</sup> Figure 5 shows the resulting band structure in the usual way of presentation, i.e., along symmetry lines only. Because the optical transitions in which we are interested are located in the  $(110)$  plane, we need the eigenvalues throughout this plane. The fcc BZ is shown in Fig. 6, with the dashed lines marking the  $(1\bar{1}0)$  and the  $(11\bar{2})$  planes, respectively. Figure 7 shows schematically the two-dimensional  $E(\vec{k})$  dependence for one valence and one conduction band, with  $\vec{k}$  restricted to the  $(1\bar{1}0)$  mirror plane. Possible transitions between these bands for one fixed photon energy are indicated by arrows. In the lower part

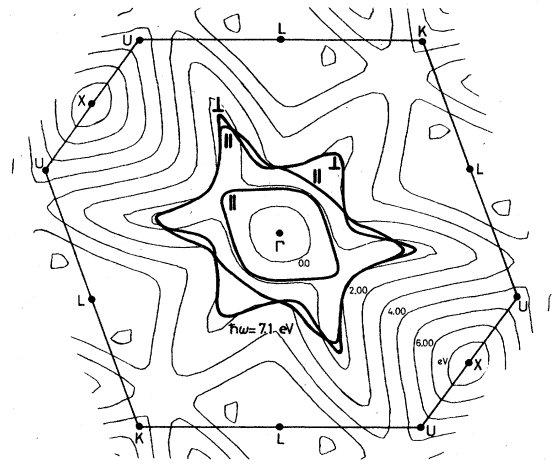


FIG. 8. Contours of constant final energy and the optical contours in the  $(1\bar{1}0)$  plane for the most important conduction band  $c_{3+}$ . The symbols  $\parallel$  and  $\perp$  indicate transitions allowed for the polarization vector parallel and perpendicular to the  $(1\bar{1}0)$  plane, respectively.

of Fig. 7, the contours of constant final energies and the optical contours of constant energy difference are shown in the  $(1\bar{1}0)$  plane. This way of representation results in energy contours, as shown in Fig. 8 for  $\hbar\omega = 7.1$  eV and for the conduction band  $c_{3+}$ , where the subscript refers to the third conduction band with the corresponding eigenfunctions having even parity with respect to the mirror reflection.

The  $\vec{k}_t$  conservation determines which fraction of the excited electrons may contribute to the  $30^\circ$  and  $60^\circ$  signals. In Fig. 9 we present a section of Fig. 8 with those regions that contribute to the experiment marked. The width of these regions is given by the angular resolution. The symbols  $\parallel$  and  $\perp$  indicate that the corresponding transitions are allowed for light polarized parallel and perpendicular to the plane of detection, respectively. Let us first concentrate on those transitions that may result in a signal at  $30^\circ$  with  $\vec{k}_t \parallel [11\bar{2}]$  (the upper one). Slightly above 0.5 eV there are transitions  $v_{2+} \rightarrow c_{3+}$  which are allowed for parallel polarized light. At about 1 eV transitions from the bands  $v_-$  and  $v_{3+}$  are possible. There are some other regions with the correct tangential component  $\vec{k}_t$  for observation in this detector, but these electrons have a group velocity directed away from the surface. For  $\bar{\theta} = 60^\circ$  and  $\vec{k}_t \parallel [11\bar{2}]$ , no transitions from the band  $v_{2+}$  are possible. At about 1 eV there are transitions from  $v_-$  and  $v_{3+}$  (left of the  $\Delta$  axis). On the right-hand side of the  $\Delta$  axis there is a small island for which electrons with kinetic energies between 0.5 and 1 eV might contribute to the  $60^\circ$  emission, originating from the same valence bands.

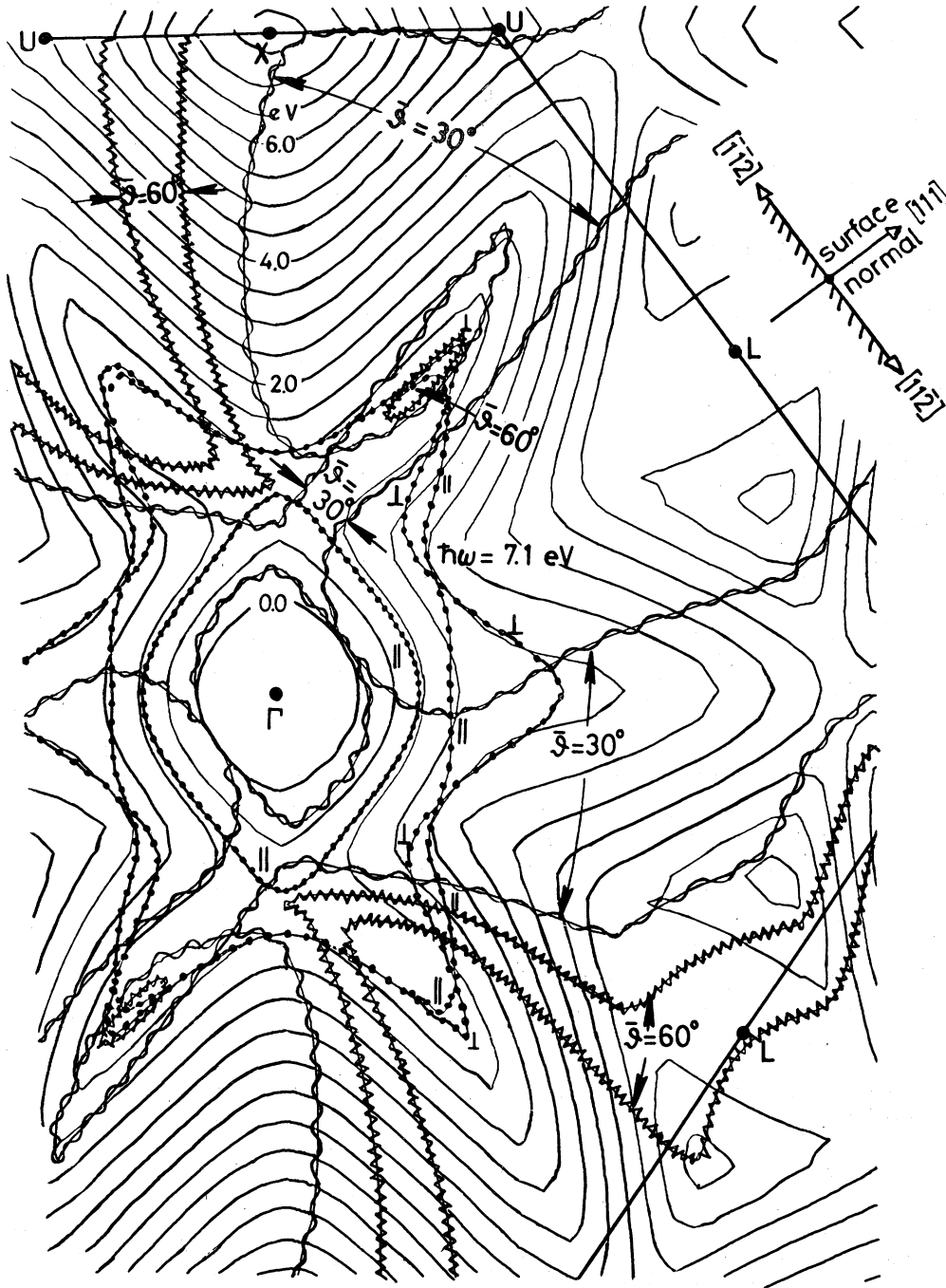


FIG. 9. Section of Fig. 8. Those regions that contribute to the signal detected in a given direction are marked. The width of these regions is determined by the angular resolution.

The situation is different for  $\bar{\vartheta} = 30^\circ$  and  $\vec{k}_i \parallel [11\bar{2}]$ . Transitions from  $v_{2+}$  are possible at about 0.8 eV. Besides this there are transitions between 1.5 and 2 eV from  $v_{3+}$  and  $v_-$ . Transitions that contribute to  $\bar{\vartheta} = 60^\circ$  and  $\vec{k}_i \parallel [11\bar{2}]$  may originate from  $v_-$  and  $v_{3+}$  between 1 and 1.5 eV. The corresponding ex-

perimental results are shown in Figs. 2 and 3.

There is a pronounced peak for  $\bar{\vartheta} = 30^\circ$  and  $\vec{k}_i \parallel [11\bar{2}]$  between 0.5 and 1 eV with the light polarized perpendicular to the plane of detection. Obviously, the transition  $v_- - c_{3+}$  is much more important than the others. To demonstrate this, we have calcu-

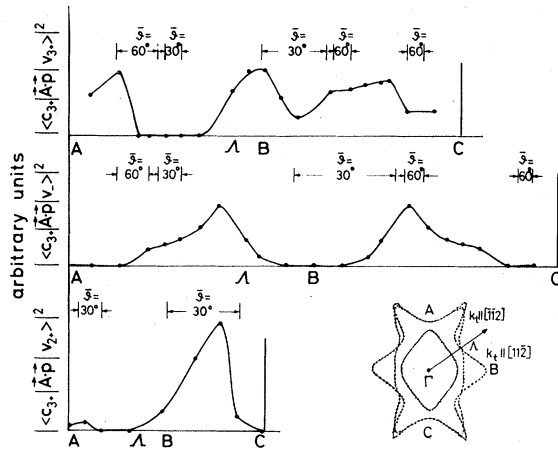


FIG. 10. Square of the transition-matrix element as a function of  $\vec{k}$  (arbitrary units). The inset shows the optical contours for  $\hbar\omega = 7.1$  eV. The variation of the transition probability is shown along these contours.

lated the expression  $|\langle f|\vec{A}^0 \cdot \vec{p}|i\rangle|^2$  from the eigenfunctions of our band-structure calculation. The result is presented in Fig. 10. The calculation is done along the optical contours from A to B to C as shown in the inset. The squared matrix elements are given in relative units. There is a strong  $k$  dependence that must be taken into account. The lower part of Fig. 10 belongs to the transition  $v_{2+} \rightarrow c_{3+}$  allowed for parallel polarization. In the middle part, the situation is shown for  $v_- \rightarrow c_{3+}$ , i.e., for perpendicular polarization. The transition probability is symmetrical with respect to the  $\Sigma$  axis in this case. The upper part is for the  $v_{3+} \rightarrow c_{3+}$  transition for parallel polarization. According to the selection rules discussed above, the matrix elements are zero for the other polarizations.

For  $\bar{\vartheta} = 30^\circ$  and  $\vec{k}_t \parallel [11\bar{2}]$  only  $|\langle c_{3+}|\vec{A}^0 \cdot \vec{p}|v_- \rangle|^2$  is of appreciable size. We therefore conclude that this transition is responsible for the dominant peak in the experiment. The weak peak for parallel polarization between 1 and 1.5 eV may be caused by the finite angular resolution perpendicular to the  $(1\bar{1}0)$  plane. We favor this interpretation because the corresponding peak in the  $(11\bar{2})$  plane proves to be very strong. Furthermore, the  $(11\bar{2})$  plane subtends only  $30^\circ$  with the  $(1\bar{1}0)$  plane. As is seen from the experimental curves for  $\bar{\vartheta} = 30^\circ$  and  $\vec{k}_t \parallel [11\bar{2}]$ , there is a strong peak between 0.5 and 1 eV and a weaker one at about 1.5 eV with parallel polarized light. Energetically the strong peak must originate from the  $v_{2+} \rightarrow c_{3+}$  transition. Moreover, the corresponding matrix element is very large in the region of interest. The matrix element for the  $v_{3+} \rightarrow c_{3+}$  transition is rather large, too. However, these elec-

trons should have a slightly higher kinetic energy. The energy differences between theory and experiment are largest in the high-energy region. The discrepancy is about 0.4 eV. This is approximately the same value by which local and non-local pseudopotential calculations differ in this energy region.<sup>10</sup> Moreover, slight misorientations of the crystal may result in a shift of the peak positions. The corresponding weak high-energy peak for perpendicular polarization is observed at slightly lower energies. This agrees with the calculations since the matrix element for the transition originating from  $v_-$  is large only where the corresponding final states are below those originating from the  $v_{3+}$  discussed above.

Let us now concentrate on the emission into  $\delta = 60^\circ$ . In this case there might be contributions into another final band, namely,  $c_{2+}$ . However, the matrix elements are small and the group velocities are almost parallel to the surface. We therefore expect the major contributions to the experimental spectra to originate also from  $c_{3+}$ . In the case of  $\vec{k}_t \parallel [11\bar{2}]$  the energy contours show that there are possible transitions on both sides of the  $\Delta$  axis. The transition probability tells us that on the left-hand side, which, by symmetry, corresponds to the  $60^\circ$  region close to the point C, only the transition  $v_{3+} \rightarrow c_{3+}$  will contribute. This transition is observed at about 1 eV, in agreement with the calculation. On the right-hand side the transition  $v_{3+} \rightarrow c_{3+}$  as well as  $v_- \rightarrow c_{3+}$  may contribute. The corresponding electrons should have energies of about 0.5 eV, again in agreement with the observed spectra. At present, however, there is no obvious explanation for the small 1-eV shoulder in the perpendicular spectrum.

In the case of  $\vec{k}_t \parallel [11\bar{2}]$ ,  $60^\circ$  we have two peaks for parallel polarization, one below 0.5 eV, the other at about 1 eV. For the perpendicular polarization there is a pronounced peak between 0.5 and 1 eV and a weak shoulder above 1 eV. According to the energy contours transitions are allowed for parallel as well as for perpendicular polarization. The corresponding transition probabilities are of equal size. The two high-energy peaks may therefore be associated with the transitions  $v_{3+} \rightarrow c_{3+}$  and  $v_- \rightarrow c_{3+}$ , respectively. The energy difference of about 0.4 eV between theory and experiment is about the same as that mentioned earlier for the  $30^\circ$  emission; it will probably be caused by the same reasons. The high-energy shoulder in the perpendicular spectrum may result from transitions into the lower final band. These transitions have the correct energetic positions and group velocities, but the corresponding calculated transition probability is rather small. The peak at 0.5 eV in the parallel spectrum may originate

from  $v_{2^*} - c_{3^*}$  transitions. According to the energy contours these transitions should not contribute to the signal. On the other hand, they adjoin the contributing region very closely. Thus a slight misorientation will bring them into a position for  $60^\circ$  emission. This interpretation is supported by the fact that this peak is badly reproducible.

An equivalent interpretation to the one presented above is successful at  $\hbar\omega = 6.5$  eV. In going from  $\hbar\omega = 7.1$  to 6.5 eV, the points of the transitions move slightly towards the  $\Gamma$  point without appreciable change in the direction of  $\vec{k}$ . The character of the final states involved does not change significantly.

#### IV. CONCLUSIONS

The prominent structure in the experimental spectra can be explained by means of a golden-rule formulation of the photoemission process, provided the transition-matrix element is calculated numerically. The commonly used assump-

tion of constant matrix elements is obviously not justified in general. We are able to interpret the gross features of the observed spectra neglecting the  $2 \times 1$  reconstruction of the surface. However, there are indications that surface states also contribute to the angular-resolved photoemission spectra even at the fairly low photon energies used in our experiments.<sup>11</sup> The surface-state emission might be responsible for the remaining differences between spectra which could be identical for the unreconstructed surface.

#### ACKNOWLEDGMENTS

We wish to thank Dr. E. Dietz for his advice and helpful discussions during the course of this investigation. We are also indebted to L. Schumacher for communicating his results prior to publication. This work is a project of the Sonderforschungsbereich 65 "Festkörperspektroskopie." The calculations were performed using the facilities of the Hochschulrechenzentrum-Universität Frankfurt.

---

\*Present address: W. C. Heraeus GmbH, D-6450 Hanau, Germany.

<sup>1</sup>H. Y. Fan, Phys. Rev. **68**, 43 (1945).

<sup>2</sup>E. O. Kane, Phys. Rev. Lett. **12**, 97 (1964).

<sup>3</sup>G. W. Gobeli, F. G. Allen, and E. O. Kane, Phys. Rev. Lett. **12**, 94 (1964).

<sup>4</sup>H. Becker, E. Dietz, U. Gerhardt, and H. Angermüller, Phys. Rev. B **12**, 2084 (1975); E. Dietz, H. Becker, and U. Gerhardt, Phys. Rev. Lett. **36**, 1397 (1976); E. Dietz and U. Gerhardt, J. Phys. F **8**, 2213 (1978).

<sup>5</sup>For example, M. M. Traum, J. E. Rowe, and N. E. Smith, J. Vac. Sci. Technol. **12**, 298 (1975).

<sup>6</sup>H. Flietner, Phys. Status Solidi **2**, 237 (1962).

<sup>7</sup>J. J. Lander, G. W. Gobeli, and J. Morrison, J. Appl. Phys. **34**, 2298 (1963).

<sup>8</sup>E. O. Kane, Phys. Rev. **175**, 1039 (1968).

<sup>9</sup>J. Hermanson, Solid State Commun. **22**, 9 (1977).

<sup>10</sup>J. R. Chelikowsky and M. L. Cohen, Phys. Rev. B **10**, 5095 (1974).

<sup>11</sup>L. Schumacher (private communication).